Intrinsic kinetics of the oxidation of methane over an industrial copper(II) oxide catalyst on a γ-alumina support

Veldsink, J.W.; Versteeg, G.F.; Swaaij, W.P.M. van

Published in:
The Chemical Engineering Journal

DOI:
10.1016/0923-0467(94)02872-8

Publication date:
1995

ELSEVIER

The Chemical Engineering Journal 57 (1995) 273–283

THE CHEMICAL ENGINEERING JOURNAL

Intrinsic kinetics of the oxidation of methane over an industrial copper(II) oxide catalyst on a γ-alumina support

J.W. Veldsink *, G.F. Versteeg, W.P.M. van Swaaij

Department of Chemical Engineering, University of Twente, P.O. Box 217, 7500 AE Enschede, Netherlands

Received 20 January 1994

Abstract

The kinetic rate of the heterogeneously catalysed methane oxidation reaction was studied at temperatures ranging from 723 to 923 K and atmospheric pressure. A commercially available CuO catalyst supported by thermally stable γ-Al_2O_3 was used as the catalyst. This kinetic study was carried out in order to evaluate whether this reaction can be suitably handled in a novel type of membrane reactor (J.W. Veldsink et al., *Chem. Eng. Sci., 47* (9–11) (1992) 2939–2944).

The equipment in which the experiments were conducted consisted of a differentially operated fixed-bed reactor. For this set-up heat and mass transport limitations have been checked and shown to be absent. The influence of the concentrations of the products and reactants on the reaction rate was studied over a wide range of conditions. Fractions of methane ranged from 1 to 6 vol.%, oxygen between 600 ppm and 21 vol.%, carbon dioxide between 0 and 20 vol.%, and water from 0 to 8 vol.%. All experimentally observed reaction rates could be represented within 30% by an Eley–Rideal type reaction rate expression.

Keywords: Reaction kinetics; Combustion; Fixed-bed reactor

1. Introduction

Natural gas is a major primary energy source in the Netherlands and owing to the large resources will continue to be in the near future. Combustion of methane is used on a wide scale, amongst other methods, to generate heat and power for industrial activities and domestic purposes. However, the relatively high flame temperatures occurring in commercial burners produce undesired amounts of NO_x. In order to reduce the total NO_x emission, research programs have been started to develop low temperature catalytic burners. Today a commercial copper(II)-oxide catalyst on La-doped γ-alumina is available and applicable for combustion of methane at a maximum temperature of 973 K [1].

Catalytic combustion of methane is a very fast and strongly exothermic reaction, which can be handled on a commercial scale in, for example, a fixed-bed or fluid-bed reactor. Owing to the thermal characteristics of this combustion reaction (rapid and excessive heat production), temperature control is very difficult in the fixed-bed reactor. Another complication is that the reactants have to be premixed at the reactor entrance. Since methane–air mixtures are liable to explode within a certain composition range, the fixed-bed catalytic methane combustor has a severely limited operation window. In the fluid-bed reactor methane conversion is limited owing to partial by-passing of the catalyst and axial mixing of the gas phase. This results in undesired methane emissions, unless an additional combustor, such as a fixed-bed, is present to convert the uncombusted methane. Other problems related to fluid bed reactors are particle attrition and erosion. These disadvantages may possibly be overcome in a new type of reactor, the catalytic membrane reactor with separated feed of reactants [2,3]. To evaluate this reactor as a combustor, the kinetics of the methane combustion reaction have to be known. This study presents the results of a kinetic study on the oxidation of methane over a commercially available CuO–γ-Al_2O_3 catalyst (Engelhard Inc.).

Only a limited amount of data has been reported on the kinetics of heterogeneous methane combustion in open literature. In order to test a great number of different catalysts in their activity towards the heterogeneous methane combustion, Anderson et al. [4] conducted conversion measurements of methane in a micro-catalytic reactor. This reactor was packed with a small volume of active catalyst material over which

* Present address: Department of Chemical Engineering, University of Groningen, Nijenborgh 4, 9747 AG Groningen, The Netherlands.

SSDI 0923-0467(94)02872-8

oxygen–methane mixtures containing only small amounts of methane, were passed. At temperatures ranging from 200 to 600 °C these authors observed a first-order rate equation with respect to methane. The activation energy over a CuO catalyst supported by γ-Al_2O_3 turned out to be $E_A = 92.4$ kJ mol^{-1}. A similar study was carried out by Malinsky [5], who passed air containing 4% methane over a catalyst bed. The relative conversion with respect to methane was always kept below 1%, in order to ensure differential behaviour and to avoid temperature gradients. Malinsky reports a first-order rate equation with respect to methane and zero-order with respect to oxygen. Furthermore, for CuO–γ-Al_2O_3 Malinsky reports a value of the activation energy $E_A = 93.7$ kJ mol^{-1}, which is close to the value of Anderson et al. [4]. Tijburg [1] developed a thermally stable γ-Al_2O_3 support by adding a small amount of lanthanum to it. The support material was impregnated with CuO as the active catalyst. At temperatures ranging from 400 to 700 °C, the heterogeneous methane oxidation reaction was studied in a micro-catalytic reactor. Tijburg presents an activation energy of $E_A = 101$ kJ mol^{-1} and a first-order rate equation with respect to methane, and zero-order with respect to oxygen.

A more rigorous kinetic study was carried out by Trimm and Lam [6], who studied the methane combustion reaction over a Pt catalyst supported by γ-Al_2O_3. These authors varied the oxygen as well as the methane concentration over a wide range. The experimentally obtained conversion data were fitted to different types of rate equation, and the best results were obtained with a dual-site Langmuir–Hinshelwood rate expression. This expression contained two oxygen adsorption sites, one site on which oxygen adsorbs diatomically (associative) and another on which monoatomic (dissociative) adsorption occurs. At higher temperatures (813 K) these authors report the formation of carbon monoxide as a reaction product.

From the literature it was concluded that no unique kinetic rate expression of methane combustion over CuO–γ-Al_2O_3 catalysts is available which describes the reaction rate over a wide temperature range, methane and oxygen partial pressures as well as the influence of the reaction products. Therefore, the reaction rate of methane over the copper catalyst had to be studied experimentally.

Determination of the mechanism and rate of a heterogeneously catalysed gas reaction requires the measuring of conversion rates over a wide range of reactor conditions. During these measurements concentration and temperature gradients over the bed should be avoided, so that the conditions to which the catalyst is exposed are known accurately. Differential operation of a fixed-bed reactor minimises the heat production and reactant consumption, so that gradients remain small. However, although this concept is simple a high analytical accuracy is demanded to calculate the reaction rate from small changes in the gas composition. Operation of such a differential packed-bed reactor with a product recycle is a suitable alternative, because recycling of the gas over the catalyst bed results in higher overall conversions without introducing gradients. Another advantage of such a reactor is that at very large recycle ratios ideally mixed behaviour is approximated, which makes the interpretation of the conversion data straightforward [7,8]. Several designs of recycle reactors with internal or external recycles of the gas flow were reviewed, amongst others, by Doraiswamy and Tajbl [9]. Yet, because most recycle reactors suffer from mechanical problems, the once-through differential fixed-bed reactor is a simple alternative at elevated temperatures.

The intention of this study is to investigate the kinetics of heterogeneous methane combustion over a CuO–γ-Al_2O_3 catalyst (Engelhard Inc.), and over a temperature range between 723 and 923 K. The influences of methane, oxygen, carbon dioxide, and water on the reaction rate were studied, in order to derive a rate expression that can be used over a wide range of reactor conditions. The reaction proceeds at elevated temperatures and the experiments are carried out in a differentially operated packed-bed reactor. Special attention was paid to possible heat and mass transfer limitations.

2. Theory

Without revealing the exact reaction mechanism, the rate of a reaction A + B → products is generally represented as a powerlaw product in the partial pressures (gas-phase reaction) of the reactants, products, and, occasionally, inert components.

$$R_A = k_r \prod_{i=1}^{n} (x_i p)^{n_i} \quad (\text{mol m}_{cat}^{-3}\ \text{s}^{-1}) \tag{1a}$$

where

$$k_r = k_0 \exp\left(\frac{-E_A}{RT}\right) \tag{1b}$$

Such an expression can be experimentally determined from conversion measurements and holds only within a specific interval of process conditions. The mass balance over the reactor relates the conversion to the reaction rate. The exact formulation of the mass balance depends on the reactor type (e.g. degree of mixing of the gas phase) used in the experiments. For a plug flow reactor and constant gas density [10] it can be derived that

$$\frac{d\zeta_A}{d\tau_{cat}} = \frac{RTR_A}{p_{A,0}} \tag{2}$$

and in case of a completely backmixed reactor

$$\tau_{cat} = \frac{p_{A,0}}{RT}\frac{\zeta_A}{R_A} \quad (3)$$

Usually, R_A is a function of the conversion. From Eqs. (2) and (3) it is clear that for a given expression of R_A only at short residence times and respective low degrees of conversions are the differences between these extreme reactor types negligible. Therefore, if the degree of mixing of the reactor used in the kinetic study is not exactly known, differential operation will be preferred.

Apart from an empirical powerlaw equation it is also possible to derive more mechanistic rate expressions. These expressions consider the basic important steps in the reaction process, such as adsorption of reactants, desorption of products, surface reaction [10,11]. The most frequently used mechanistic rate equations are the Langmuir–Hinshelwood, Eley–Rideal, and reduction–oxidation rate expression. The next paragraph gives a brief discussion of these types of expression.

The Eley–Rideal mechanism considers only adsorption of component A on the catalyst, which reacts with gaseous B. The elementary steps of this mechanism are as follows.

(1a)	A_2 (gas) $\rightarrow$ A_2 (ads)	(associative, molecular adsorption)
(1b)	A_2 (gas) $\rightarrow$ 2A (ads)	(dissociative adsorption)
(2)	A_2 (ads) + B (gas) $\rightarrow$ R (ads) + S (ads)	(surface reaction)
(3)	R (ads) $\rightarrow$ R (gas)	(desorption of products)
(4)	S (ads) $\rightarrow$ S (gas)	

The surface reaction (step 2) is assumed to be the rate controlling step and the adsorption and desorption steps are at equilibrium. Under steady-state conditions reaction rate expression can be derived, resulting in

$$R_A = \frac{k_r(K_A p_{A2})^q p_B}{1 + (K_A p_{A2})^q + K_R p_R + K_S p_S + K_I p_I} \quad \text{(ER)} \quad (4)$$

with $q = 1$ in case of associative or 0.5 in case of dissociative adsorption; K adsorption constant of reactants, products and inert gases respectively; k_r first order reaction rate constant (see Eq. (1b)); p_i partial pressure of component i.

The denominator also takes the adsorption of inert species into account, because this reduces the catalyst activity by occupation of active sites.

When component B should also adsorb on the surface before the reaction can proceed, the process is known as the Langmuir–Hinshelwood mechanism. Now the elementary steps become

(1)	A_2 (gas) $\rightarrow$ A_2 (ads) (or A_2 (gas) $\rightarrow$ 2A (ads))
(2)	B (gas) $\rightarrow$ B (ads)
(3)	A_2 (ads) + B (gas) $\rightarrow$ R (ads) + S (ads)
(4)	R (ads) $\rightarrow$ R (gas)
(5)	S (ads) $\rightarrow$ S (gas)

Based on the same assumptions as the Eley–Rideal mechanism the kinetic rate expression reads

$$R_A = \frac{k_r(K_A p_{A2})^q K_B p_B}{(1 + (K_A p_{A2})^q + K_B p_B + K_R p_R + K_S p_S + K_I p_I)^2} \quad \text{(LH)} \quad (5)$$

Another mechanism sometimes observed in heterogeneous oxidation reactions is the Mars and van Krevelen reduction–oxidation mechanism (see Ref. [12]). This mechanism assumes that lattice oxygen of the catalyst itself is involved in the oxidation step and replaced afterwards by gaseous oxygen. According to this mechanism the reaction rate is expressed as

$$R_A = \left(\frac{1}{k_r p_B} + \frac{1}{K_{A2} p_{A2}}\right)^{-1} \quad \text{(Red–Ox)} \quad (6)$$

Asymptotic cases of Eqs. (4)–(6) lead to reaction rate expressions like Eq. (1a), holding only for a specific interval of partial pressures and process conditions. If, for instance, the rate of a reaction is given by Eq. (5) (LH-scheme) and only adsorption of component A is important, this expression will reduce to ($q = 1$)

$$R_A = \frac{k_r(K_A p_{A2})K_B p_B}{(1 + (K_A p_{A2}))^2}$$

At high partial pressures of A, the rate dependence on component A may become reciprocal to p_A ($K_A p_A \gg 1$):

$$R_A = k_{app} p_B p_A^{-1}$$

whereas at low partial pressures of A a linear proportionality in A might be observed:

$$R_A = k_{app} p_B p_A$$

Starting from the ER (Eq. (4)) or red–ox mechanism (Eq. (6)) results in other asymptotic rate expressions. Therefore, the asymptotic behaviour of the experimentally determined rate equation enables discrimination between the mechanistic models.

3. Transport limitations

The conversion rate is not necessarily controlled by the rate of the intrinsic reaction process alone, but also the transport rate of components to and from the external catalyst surface and diffusion inside the pores may affect the experimentally observed rate. When dealing with endo/exothermic reactions heat transport may also be important, because heat transfer limitations give rise to temperature gradients over the catalyst bed or between the gas phase and catalyst. When steep gradients are present, the reaction rate, which generally

depends strongly on temperature, may differ from particle to particle. Therefore, transport limitations of heat and mass have to be checked for the experiments in order to exclude these effects on the overall conversion rate.

3.1. Mass transport

The conversion rate in a porous catalyst is a result of the rates of mass transport to the external catalyst surface and diffusion and reaction inside the catalyst pore structure. Under steady-state conditions, the molar flux J_A of the (reacting) components at the external catalyst surface should be equal to the conversion rate inside the catalyst particle. For a spherical particle at isothermal conditions this is expressed as

$$J_A = \frac{k_g}{RT}(p_A - p_{A,i}) = R_A(p_{A,i})\frac{d_p}{6}\eta \tag{7}$$

with k_g the gas-to-particle mass transport coefficient ($m\,s^{-1}$), d_p the particle diameter (m); η the effectiveness factor.

First, Eq. (7) shows that only in the case of a sufficiently high mass transport coefficient does the interfacial partial pressure $p_{A,i}$ approximately equal the gas bulk partial pressure. In this case the reaction rate can be expressed in terms of the measurable quantity p_A instead of $p_{A,i}$. Secondly, the effectiveness factor of the catalyst pellet should equal unity to ensure that the reaction proceeds at uniform conditions. The effectiveness factor is defined as the ratio of the average reaction rate over the reaction rate at conditions prevailing at the surface of the catalyst particle [10]:

$$\eta = \frac{1}{V_{cat}R_A(p_{A,i})}\int_{V_{cat}} R_A(p_A)\,dV \tag{8a}$$

According to this definition a value of unity generally means that there is a full utilization of the internal area of the catalyst and internal concentration gradients are absent. Internal transport limitations have to be considered at a value less than unity. For a general nth-order reaction Eq. (8) can be rewritten as a function of the Thiele modulus ϕ:

$$\eta = \frac{1}{3\phi^2}\left(\frac{3\phi}{\tanh(3\phi)} - 1\right) \tag{8b}$$

with

$$\phi = \frac{d_p}{6}\left[\frac{(n+1)k^n RT}{2D_A^{eff}}p_{A,i}^{n-1}\right]^{1/2} \tag{9}$$

To ensure that the effectiveness factor approximates unity, the value of the Thiele modulus ϕ must be evaluated and should be less than 0.3. If a series of experiments results in $\phi > 0.3$, the experiments have to be repeated with, for instance, a smaller particle size.

3.2. Heat transport

As mentioned before, the reaction rate constant often depends on the temperature according to an Arrhenius relation (Eq. (1b)), and if the catalyst bed is not at isothermal conditions, the observed reaction rate will be an averaged result of different local reaction rates. Owing to the fact that the combustion of methane is a very exothermic reaction, a high heat transport rate should be accomplished to avoid severe temperature gradients. Transport of heat can be distinguished on three levels, the intraparticle transport, occurring inside the catalyst particle, interparticle transport of heat between adjacent particles in the bed, and interphase transport between the solid catalyst particle and the gas phase. At each of these levels transport limitations are possible and have to be checked.

Several authors have derived criteria which can be used to estimate the effect of the various heat transport limitations [13,14].

(1) Intraparticle gradients will not have influenced the conversion rate by more than 5% if

$$\frac{|\Delta H|R_A d_p^2 E_A}{4\lambda_{cat}RT_{cat}^2} < 1 \tag{10}$$

is fulfilled during the experiments.

(2) Heat transfer limitation between adjacent particles in the catalyst bed (interparticle gradients) results in a temperature profile over the catalyst bed. In a fixed-bed reactor with a cooled wall the radial temperature profiles are approximately parabolic, whereas the fluid temperature along the axis rises to a maximum at the 'hot spot', before gradually returning to the wall temperature. The maximum dimensionless temperature difference θ_{rad} between the hot spot temperature T and the reactor wall temperature T_w can be estimated from

$$\theta_{rad} \equiv \frac{E_A(T-T_w)}{RT_wT_w} = \frac{|\Delta H|R_A(1-\epsilon)d_0^2E_A[1+16(d_p/d_0)Bi_h}{1.6(1+b)RT_w^2\lambda_{eff}} \tag{11}$$

with

$$Bi_h = \frac{\alpha_w d_p}{2\lambda_{eff}}$$

If relation (11) is fulfilled during the experiments, the rate at the hot spot will not differ by more than 5% from the rate at wall conditions. At differential operation, however, it is unlikely that the gas will reach the hot spot temperature. Therefore, applying this relation to the differentially operated fixed-bed reactor yields an overestimated interparticle temperature gradient.

(3) Laboratory reactors are sensitive to temperature gradients over the gas film surrounding the catalyst

particle (interphase gradients), because the flow rates are usually low. The maximum interphase temperature gradient can be calculated by solving the heat balance over a catalyst particle assuming that all heat is transferred through the gas phase:

$$\frac{R_A}{a_s}|\Delta H| = \alpha(T_{cat} - T_{gas}) \tag{12}$$

The heat transfer coefficient α can be estimated by [15]

$$\frac{\epsilon k_g}{v_g}\left(\frac{\nu}{D}\right)^{2/3} = 0.81\left(\frac{v_g d_p}{\nu}\right)^{-0.5} \quad \text{for } 5 < Re_p < 500 \tag{13}$$

Using the Chilton–Colburn analogy of heat and mass, from the value of the mass transport coefficient a value of the heat transport coefficient can be obtained:

$$\frac{\alpha}{k_g} = \rho c_p \left(\frac{\lambda}{\rho c_p D_A^0}\right)^{2/3} \tag{14}$$

The value of the heat transfer coefficient obtained from Eqs. (13) and (14) includes no contribution of natural convection or radiation, and, therefore, it can be regarded as a conservative estimate.

4. Experimental set-up

Fig. 1 shows the experimental set-up which consists of a small tubular quartz reactor (ID 7×10^{-3} m) with a bed (4×10^{-3} m < height < 5×10^{-3} m) of catalyst and dilution material ($1.5 \leqslant b \leqslant 20$). Catalyst particles of several mesh sizes (100 μm < d_p < 125 μm, 150 μm < d_p < 212 μm and 600 μm < d_p < 710 μm) were used in the experiments. As a dilution material α-alumina was available at mesh sizes $d_p < 500$ μm, whereas SiC was available at 500 μm < d_p < 1000 μm. Inside the bed a thermocouple (K-type) monitored its temperature, and a surrounding temperature controlled fluid sand-bed provided a quick and stable temperature control of the system. Inlet gas compositions (methane (0–6%), carbon dioxide (0–15%), oxygen (0–20%)) were set and controlled by thermal mass flow controllers ($\phi_v \leqslant 3.6\times10^{-5}$ Nm^3 s^{-1}). Water was added to the gas flow by saturating the gas flow in a temperature controlled bubble column. Before coming into contact with the catalyst bed the gas mixture was preheated over a quartz wool section, present in the quartz tube.

Immediately after leaving the catalyst bed the gas mixture was quenched, dried, and fed to an analyzer section consisting of an infrared CO_2-analyzer and a gas chromatograph. For all experiments mass balances were checked in order to detect any side reactions.

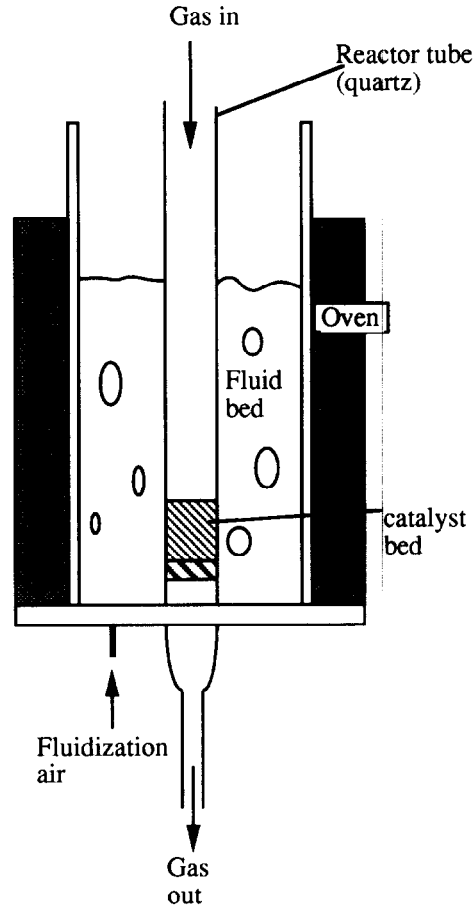

Fig. 1. Schematic representation of the differential packed bed reactor.

5. Preliminary system checks

When a mixture of dry air containing 5% methane was passed through the empty reactor, methane conversion was not observed ($\zeta < 10$ ppm) up to 725 °C. Packing the reactor with a bed of inert material (quartz wool, α-alumina, SiC) also showed no detectable conversion when this gas mixture was passed through. The temperature over the packed bed of inert material (height 0.01 m) was constant in the axial direction over its whole height. Furthermore, it was verified that the length of the preheating zone was sufficient to ensure that the gas mixture entered the bed at reaction temperature.

Before starting the kinetic experiments, it was checked that the catalyst showed a stable activity over a sufficiently long period of time at 550 °C. After a small initial loss the catalyst activity remained practically constant. The loss of activity was below 1% over a period of two hours, when kept under an oxidizing as well as a reducing gas atmosphere. During the night the catalyst was exposed to dry air at reaction temperature. At 650 °C and a high water content of the gas stream, fastest deactivation of the catalyst was observed, and the catalyst lost about 3% of its activity

per hour. This is explained by some sintering or conversion of γ-alumina to α-alumina occurring at higher temperatures [1]. Nevertheless, at all temperatures the catalyst remained stable over a sufficiently long period to carry out a series of experiments. At the beginning and end of each series of experiments, the conversion of a reference experiment (5% methane, balance air) was measured to check the activity of the catalyst. In case the conversion of this reference experiment was observed to be less than 95% of the initial conversion, the catalyst was replaced with fresh material. After it was verified that the fresh catalyst had passed its initial decrease in activity, the experiments were continued.

From these initial experiments it was concluded that the experimental set-up was suitable to obtain reliable conversion data of the methane combustion over the $CuO-\gamma-Al_2O_3$ catalyst.

6. Results and discussion

6.1. Influence of methane on the reaction rate

The experiments were started with gas mixtures of dry air containing variable amounts of methane (0–6%). These experiments with excess oxygen allowed us to determine the reaction rate as a function of the methane partial pressure, because during an experiment the oxygen pressure remained constant. Fig. 2 shows the observed reaction rate as a function of the partial pressure of methane at 923 K. Similar results were obtained at other temperatures (723 K $\leqslant T \leqslant$ 923 K), and a first-order behaviour of methane was observed in all cases.

According to these experiments, the reaction rate can be expressed as (see Eq. (1))

$$r_A = k_{app}(T, p_{O2})p_{CH4} \quad (\text{kmol kg}_{cat}^{-1}\ \text{s}^{-1}) \qquad (15)$$

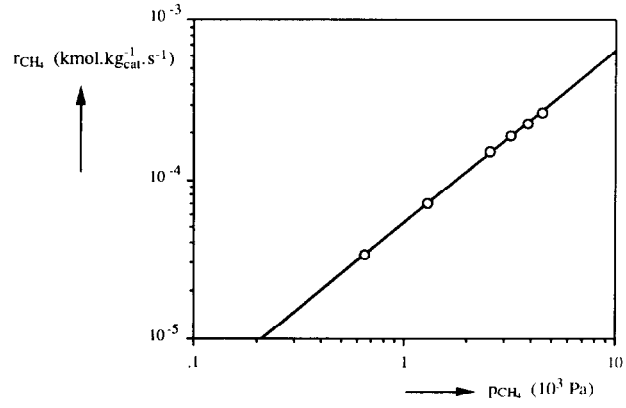

Fig. 2. Rate dependence on the methane partial pressure in excess oxygen. Conditions: $T_{wall} = 923$ K, 920 K $\leqslant T_{bed} \leqslant$ 932 K, $p_{O2} = 22$ kPa, $v_g = 3.1$ m s^{-1}, 150 μm $< d_p <$ 212 μm, $b = 16$.

In Eq. (15) an apparent reaction rate constant is introduced, because it depends not only on temperature, but is a function of the partial pressure of oxygen and other components as well. Since the oxygen partial pressure was the same and constant during all experiments, the temperature dependence can be obtained from Fig. 3 where the apparent reaction rate constant is given as a function of temperature according to Eq. (1a). An apparent activation energy of $E_A = 135$ kJ mol^{-1} was derived, being somewhat higher than those reported in open literature. Malinsky [5], who studied the reaction rate of methane combustion over $CuO-\gamma-Al_2O_3$ in excess of oxygen found a value of $E_A = 94$ kJ mol^{-1}, Anderson et al. [4] found $E_A = 93$ kJ mol^{-1}, and Tijburg [1], for the same catalyst as used in the present experiments, observed a value of $E_A = 101$ kJ mol^{-1}.

The experimental results obtained so far could be used as input parameters in the equations to check for any transfer limitations, discussed in Section 3. Apart from the kinetic data, physical data are also needed in the equations and these are summarized in Table 1. For the values of the gas viscosity, thermal conductivity and heat capacity, the equivalent values

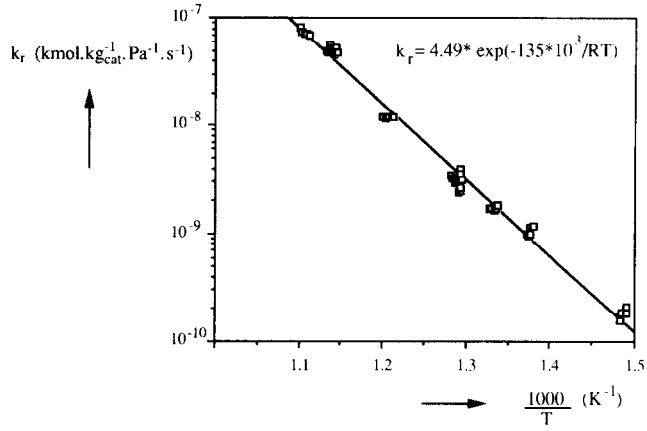

Fig. 3. Arrhenius plot of the oxidation kinetics of methane combustion in excess oxygen.

Table 1
Physical properties of the catalyst material and reaction system

$CH_4 + 2O_2 \rightarrow CO_2 + 2H_2O$
$\Delta H_r = -8.03 \times 10^5$ (J mol^{-1})
$D^0_{ethane,\ air} = 0.88 \times 10^{-4}$ (m^2 s^{-1}, at 773 K, 0.13 MPa)
$D^0_{oxygen,\ air} = 1.08 \times 10^{-4}$ (m^2 s^{-1}, at 773 K, 0.13 MPa)
$\lambda_{cat} = \lambda_{\gamma\text{-alumina}} \approx 8$ (W m^{-1} K^{-1})
$\epsilon_{bed} = 0.43$
$D^{eff}_{Z-A} = 0.1 D_A$
$r_p = 7.2 \times 10^{-9}$ (m)
$\rho_{cat} = 1040$ (kg m$^{-3}_{cat}$)
$V_{pore} = 0.78$ (cm^{-3} g^{-1})
Area = 163.6 (m^2 g^{-1})

of air were taken, which are given as a function of temperature by the International Critical Tables of the National Research Council [16].

The value of the particle-to-fluid mass transfer coefficient was estimated from Eq. (13). Substitution of this value together with the measured methane flux in Eq. (7) showed that the interfacial partial pressure of methane was very close (within 5%) to the bulk partial pressure for all experiments. Therefore, particle-to-fluid mass transfer did not hamper the kinetic measurements. Additional experimental checks were carried out by studying the conversion as a function of the superficial gas velocity. While the superficial gas velocity was decreased by over two orders of magnitude, the conversion rate remained constant. Since the value of the gas-to-particle mass transfer coefficient depends on the gas velocity, the absence of external mass transfer limitations could be concluded from these experiments. However, during these experimental checks Re_p decreased over the same range and, hence, Eq. (13) does not hold over the full range. Moreover, the exact dependence of the mass transfer coefficient on the gas velocity at $Re_p \ll 1$ is still not clear. Some authors have found that the mass transfer coefficient depends strongly on the gas velocity at low Re numbers, whereas others (see Ref. [17]) consider that the value of k_g becomes relatively independent of the gas velocity. However, for all kinetic experiments $Re_p > 5$, so it was concluded that mass transfer limitations ($< 5\%$) were absent.

According to Eq. (15) the reaction rate expression is first order, so the Thiele modulus (Eq. (9)) reduces to

$$\phi = \frac{d_p}{6}\left(\frac{k_{app}}{D_A^{eff}}\right)^{1/2} \tag{16}$$

From the experimental rate data it was concluded, using Eq. (16), that always $\phi < 0.3$ and hence $\eta \approx 1$. In the previous section, the absence of external mass transfer limitations was already concluded, so that from Eq. (7) it can be concluded that the measured flux represents the kinetic rate.

The temperature difference between gas phase and particle was calculated using Eqs. (12)–(14). The measured reaction rate, corrected by the catalyst density, was substituted for R_A, and the reading of the thermocouple in the catalyst bed was assumed to represent the gas temperature. Eq. (12) then allows the catalyst particle temperature to be calculated as a function of transfer coefficients, average reaction rate, and gas-phase temperature. Fig. 4 shows the calculated particle temperature as a function of the gas temperature for all experimentally observed reaction rates and no severe

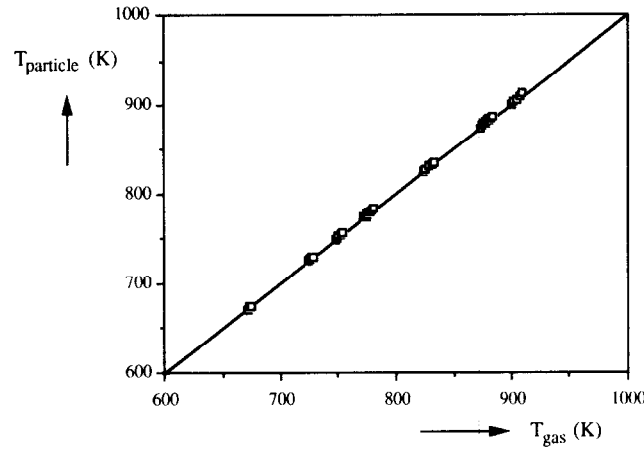

Fig. 4. Calculated particle temperature according to Eq. (12) as a function of the measured gas temperature.

temperature differences between gas and catalyst particle.

The effect of intraparticle temperature gradients turned out to be negligible from Eq. (10). The thermocouple readings inside the catalyst bed were always close to the wall temperature, so that severe temperature gradients over the bed were not observed. Furthermore, Eq. (11), presenting a worst-case analysis for the differentially operated fixed bed reactor, held for nearly all experiments.

To be able to operate at low conversion levels the amount of active catalyst had to be very small. Therefore, either the height of the catalyst bed should be kept very low (in the present study approximately 1–2 particle layers), or the active catalyst should be mixed with inert material. In both cases the distribution of catalyst over the bed could affect the conversion, as indicated by van den Bleek et al. [18]. However, at low conversion levels (and ideal mixing) this effect of catalyst distribution disappears and according to the criteria of van den Bleek et al. appeared to be less than 1.5% under the present conditions.

Finally, carbon mass balances were observed to match within 5% in all cases, and, because no detectable amounts of carbon monoxide were observed, it was concluded that the reaction proceeds according to, $CH_4 + 2O_2 \rightarrow CO_2 + 2H_2O$. Under the experimental conditions, the reduction–oxidation mechanism seems unlikely as a possible reaction mechanism, because the methane reaction order did not change and remained first order, even at reduced oxygen partial pressures.

6.2. Influence of oxygen

At constant methane pressures, the influence of oxygen on the intrinsic rate was studied, and the results at low temperatures are shown in Fig. 5. The reaction rate was first order with respect to methane, so Fig. 5 presents the ratio of the reaction rate over the methane partial pressure as a function of the oxygen pressure.

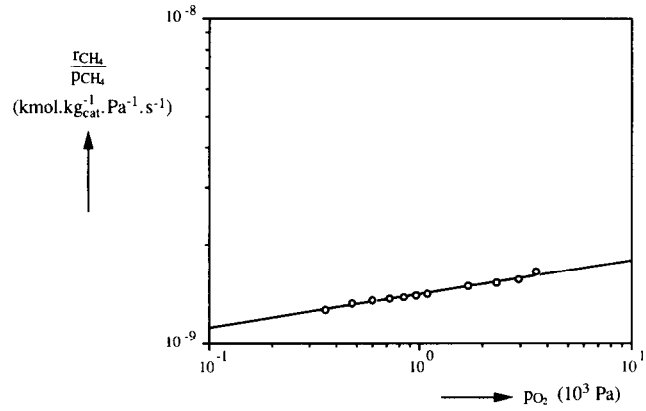

Fig. 5. Reaction rate dependence on oxygen. Experimental conditions: $T_{wall}=750$ K, 750 K$\leqslant T_{bed}\leqslant$752 K, $p_{CH4}=6.5$ kPa, $v_g=2.1$ m s^{-1}, 600 μm$<d_p<$710 μm, $b=16$.

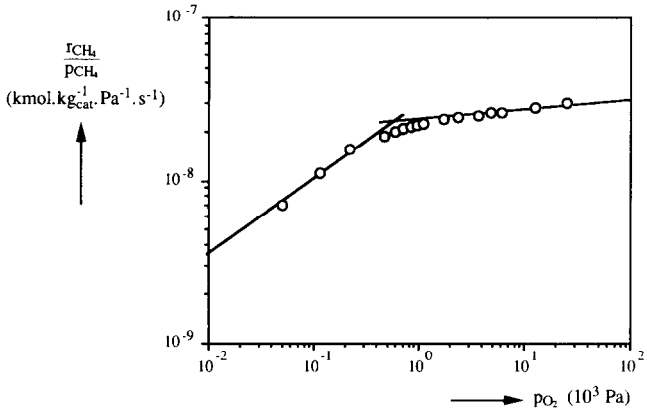

Fig. 6. Reaction dependence on oxygen. Experimental conditions: $T_{wall}=873$ K, 872 K$\leqslant T_{bed}\leqslant$880 K, $p_{CH4}=6.5$ kPa, $v_g=2.5$ m s^{-1}, 150 μm$<d_p<$212 μm, $b=16$.

From Fig. 5 it could be concluded that the reaction order with respect to oxygen was $n=0.07$. However, at higher temperatures a change in the rate dependence on oxygen was observed, which is shown in Fig. 6. At high partial pressures the kinetic rate becomes fairly independent of oxygen and changes to a square root proportionality at low oxygen pressures.

From the results of Figs. 5 and 6, it can be concluded that the influence of oxygen on the reaction rate is not straightforward, and that probably adsorption phenomena have to be taken into account. Therefore, Eq. (1) cannot be used to represent the reaction rate over a broad range of oxygen pressures. More likely expressions analogous to Eqs. (4)–(6) have to be used to cover all the experimental results in a unique rate expression. For all experiments, the reaction order with respect to both oxygen and methane appeared to be positive, and a maximum was not observed in the reaction rate versus partial pressure diagrams. Hence, there is no indication that the Langmuir–Hinshelwood expression should be used to represent the kinetic data. The Eley–Rideal mechanism (Eq. (5)) seems suitable to describe the experimental data. The half-order rate equation with respect to oxygen at low partial pressures can be interpreted as dissociative adsorption of oxygen.

6.3. Influence of carbon dioxide

At constant partial pressures of oxygen and methane, CO_2 fractions were varied between 0% and 15%. Fig. 7 shows the ratio of the reaction rate over the methane partial pressure as a function of the CO_2 partial pressure, and a small negative influence of CO_2 is observed. Experiments at various temperatures, 673 K$\leqslant T\leqslant$973 K, resulted in similar diagrams, showing always a negative apparent CO_2 order of approximately 0.1. Apparently, CO_2 adsorbs at the same sites as oxygen and reduces the number of available active sites, although its influence is rather small.

The experimental data on the CO_2 dependence are less accurate because the conversion was calculated from the produced amount of CO_2 detected in the outlet gas flow by means of an infrared analyzer. In case the feed stream already contains carbon dioxide, the conversion had to be obtained from the difference between inlet and outlet gas stream.

6.4. Influence of water

Finally, the influence of water on the reaction rate was studied. Inlet gas streams of air, containing variable amounts of methane, were passed through a bubble column filled with water, and saturated before entering the catalyst bed. The water content was varied by changing the operating temperature of the bubble column. Fig. 8 presents a plot of the apparent reaction rate as a function of the methane partial pressure at different inlet water pressures. The order of methane appeared to be unity, as in the dry experiments. The reaction rate decreases when the feed was saturated with water at a higher temperature, so that water has a negative influence on the reaction rate. Plotting the

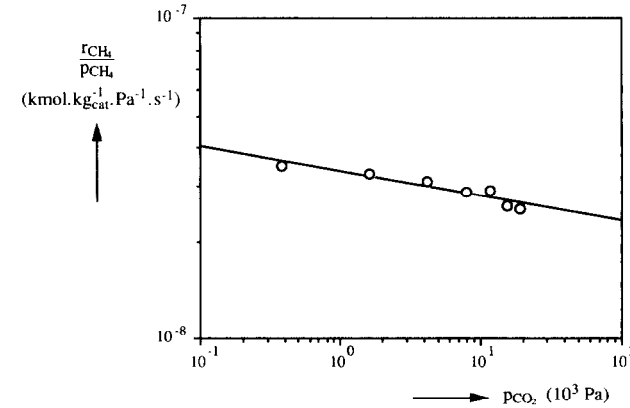

Fig. 7. Dependence of the reaction rate on carbon bioxide. Experimental conditions: $T_{wall}=873$ K, 872 K$\leqslant T_{bed}\leqslant$880 K, $p_{CH4}=3.7$ kPa, $p_{O2}=25$ kPa, $v_g=1.7$ m s^{-1}, 150 μm$<d_p<$212 μm, $b=10$.

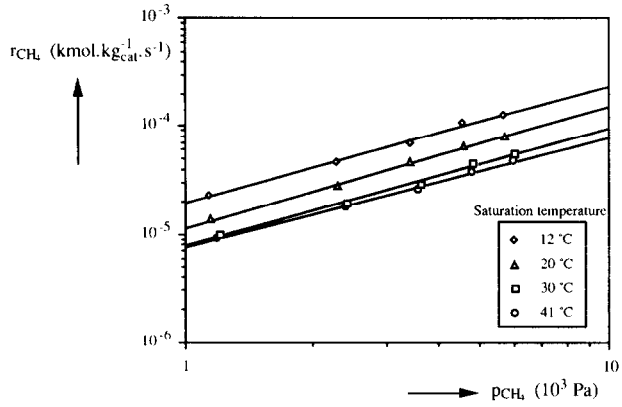

Fig. 8. Reaction rate as a function of methane pressure. Reactor feed stream was saturated with water at different temperatures. Experimental conditions: $T_{wall}=873$ K, 863 K$\leqslant T_{bed}\leqslant$883 K, $p_{O2}=25$ kPa, $v_g=1.7$ m s^{-1}, 125 μm$<d_p<$150 μm, $b=16$.

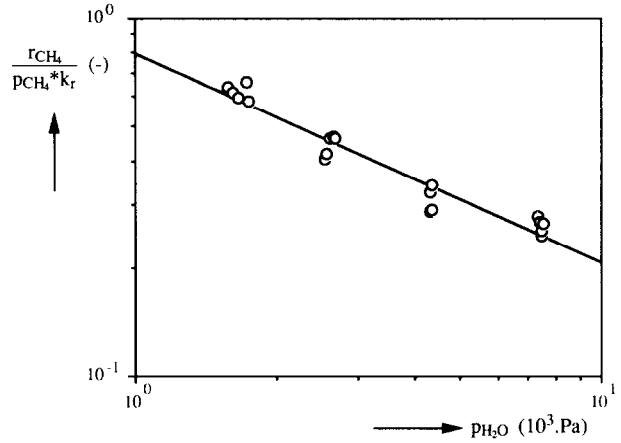

Fig. 9. Dependence of the reaction rate on water. Experimental conditions as in caption to Fig. 8.

ratio of the reaction rate over the methane pressure as a function of the water pressure shows the influence of water. Keeping the wall temperature constant, it was observed that the catalyst-bed temperature decreased a little when the water concentration was increased. The data are corrected for this (small) effect by using the estimated apparent activation energy and dividing the reaction rate to methane pressure ratio by the value of the reaction rate constant obtained from Fig. 3. The collective results are shown in Fig. 9 and similar diagrams were obtained at temperatures ranging from 723 K to 923 K. The order of the reaction rate with respect to water was found to be $-0.6\leqslant n\leqslant -0.5$.

6.5. Final rate equation of the oxidation of methane over CuO–γ-Al_2O_3 catalyst

Based on the experimental results obtained in the previous sections, it was concluded that the ER-expression (Eq. (6)) is able to describe the observed phenomena. In this rate expression a number of constants (reaction and adsorption) are present, all depend on the temperature according to an Arrhenius relation (Eq. (1a)). Owing to this large number of parameters their values are difficult to determine independently. Hence, it is useful to reduce the total number, in order to achieve a more reliable set of values.

All experiments presented were in large excess (75–95%) of nitrogen, being an inert species, so the influence of inert adsorption on the reaction rate could not be estimated properly, because the influence of nitrogen remained practically constant. Hence, the term describing the inert adsorption was excluded from the final rate expression. Secondly, the methane adsorption term was eliminated from Eq. (6), because under the experimental conditions the reaction rate appeared always to be proportional to the methane pressure. Probably, methane was too weakly adsorbed to observe any significant influence, and, therefore, this term could not be estimated accurately from the available experimental data. For a further and final reduction of the number of parameters, it was assumed that the adsorption of all components was independent of temperature. For the experiments presented, the order of a particular component has been found to depend almost on its partial pressure only, so that within the experimental accuracy this last approximation seems legitimate. The final rate expression is now reduced to a total number of five parameters:

$$r_A=\frac{k_0\exp(-E_A/RT)(0.5)(K_p)_{O_2})^{0.5}p_{CH_4}}{(1+(0.5(Kp)_{O_2})^{0.5}+(Kp)_{CO_2}+(Kp)_{H_2O})} \quad (17)$$

The numerical values of the different constants were estimated with the commercially available SIMUSOLV® package (Rapid Data Ltd.). Initially, the values of the parameters were estimated independently of one another from the experiments presented in the previous sections. From the measurements of the reaction rate as a function of the methane pressure in excess oxygen, initial values of the reaction rate constant and the activation energy were obtained. Initial values of the adsorption constants of oxygen, carbon dioxide, and water were obtained from the measurements of the reaction rate as a function of the partial pressure of oxygen, carbon dioxide, and water respectively. These parameters were taken as the initial guesses, and a final parameter optimization has been done using all experimental data. The optimized parameter values obtained from this procedure are given in Table 2. A parity plot of the calculated reaction rate according to Eq. (17) with this set of parameters and the experimentally observed rate is shown in Fig. 10. From this diagram it could be concluded that Eq. (17) is able to predict the reaction rate within approximately 30% over a wide range of conditions.

Table 2
Optimal parameter values for use in Eq. (17)

$k_0 = 1.08$ (kmol kg_{cat}^{-1} Pa^{-1} s^{-1})
$E_A = 1.25 \times 10^5$ (J mol^{-1})
$K_{O2} = 1.2 \times 10^{-2}$ (Pa^{-1})
$K_{H2O} = 1.2 \times 10^{-3}$ (Pa^{-1})
$K_{CO2} = 5.0 \times 10^{-3}$ (Pa^{-1})

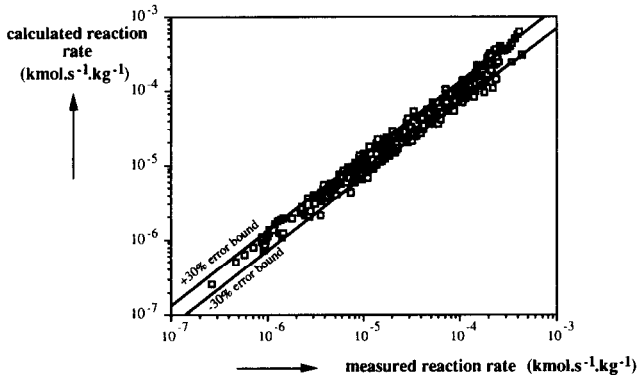

Fig. 10. Parity plot of measured reaction rate and calculated reaction rate according to Eq. (17) and parameters as in Table 2.

An attempt has also been made to fit the experimental data to the red–ox rate expression, but no suitable values of the various constants could be obtained in this case.

7. Conclusions

The intrinsic reaction rate of methane combustion under industrially important conditions can be measured in a differentially operated packed-bed reactor without any heat and mass transfer limitations. For this combustion reaction a commercially available CuO–γ-Al_2O_3 catalyst was used, which remained stable over a long period of time and at temperatures up to 923 K. Over a wide range of temperature and gas phase compositions the reaction rate was studied and a kinetic rate equation was derived covering all experimental data. Within the experimental accuracy no partial oxidation products have been observed.

The final rate equation is of the Eley–Rideal type with adsorption of oxygen, carbon dioxide, and water and no adsorption of methane on the catalyst surface. The rate equation with optimized parameter values is

$$r_{CH_4} = \frac{1.08 \exp^{-125 \times 10^3/RT}(0.6 \times 10^{-2} p_{O_2} p_{CH_4})^{1/2}}{1 + (0.6 \times 10^{-2} p_{O_2})^{1/2} + 5.0 \times 10^{-3} p_{CO_2} + 9.5 \times 10^{-3} p_{H_2O}} \quad (\text{kmol } kg_{cat}^{-1}\ s^{-1})$$

This equation is able to describe the intrinsic reaction rate of the methane combustion over a thermally stable CuO–γ-Al_2O_3 catalyst under industrially important conditions, $p_{CH_4} \leqslant 6$ kPa, $0.06 \leqslant p_{O_2} \leqslant 22$ kPa, $p_{CO_2} \leqslant 20$ kPa, $p_{H_2O} \leqslant 8$ kPa and $723\ \text{k} \leqslant T \leqslant 923$ K. A first order in methane was observed, which is in agreement with previous studies [1,4,5]. However, this study presents an activation energy of $E_A = 125$ kJ mol^{-1}, which exceeds the previously reported values. The experimental set-up used in this study, consisting of a differentially operated packed-bed, is well-suited for obtaining relevant kinetic data on the heterogeneously catalysed methane oxidation reaction.

Acknowledgements

These investigations were financially supported by Gastec, Apeldoorn, whom we gratefully acknowledge. For their contribution in the experimental part we would like to thank T.B. Duzijn and E. Veenendaal. The technical assistance of K. van Bree and A. Schanssema was also greatly appreciated.

Appendix A: Nomenclature

a_s	specific interfacial area of the catalyst (m^2 m^{-3}) ($6/d_p$ for spherical particles)
b	volumetric ratio of inert dilution material over the active catalyst (–)
Bi_h	Biot number
c_p	heat capacity (J kg^{-1} K^{-1})
d_p	particle diameter (m)
d_0	reactor diameter (m)
D_A	diffusion coefficient of component A (m^2 s^{-1})
E_A	activation energy (J mol^{-1})
ΔH	reaction enthalpy (J mol^{-1})
J_A	molar flux of A (J m^{-2} s^{-1})
k_g	gas-to-particle mass transport coefficient (m s^{-1})
k_r	reaction rate constant, units depend on the rate expression
k_0	pre-exponential value of the rate constant, see Eq. (1)
K_A	adsorption constant of component A (Pa^{-1})
n	order of reaction, see Eq. (1)
p	absolute pressure (Pa)
p_A	partial pressure of component A (Pa)
r	particle radius, (see Eq. (8)) (m)
r_A	reaction rate with respect to component A (kmol kg_{cat}^{-1} s^{-1})
R	universal gas constant (J mol^{-1} K^{-1})
R_A	reaction rate with respect to component A (mol m_{cat}^{-3} s^{-1})
T	temperature (K)
v_g	superficial gas velocity at actual conditions (m s^{-1})
x_A	mole fraction of component A (–)

Greek letters

α heat transfer coefficient (W m^{-2} K^{-1})
ϵ porosity (–)
ϕ_V volumetric flow rate (m^3 s^{-1})
ϕ $\frac{d_p}{6}\left(\frac{k_r}{D_A^{eff}}\right)^{1/2}$ (Thiele modulus, first order reaction)
η effectiveness factor
λ (effective) conductivity (W m^{-1} K^{-1})
ν kinematic viscosity (m^2 s^{-1})
θ_{rad} dimensionless temperature difference between the hot spot and the wall temperature, Eq. (11)
ρ density (kg m^{-3})
τ residence time (s)
ζ_A relative conversion with respect to component A (–)

Subscripts and superscripts

app apparently
cat catalyst
eff effective
i interface
I inert species
w wall
0 initial conditions or gas phase

References

[1] I.I.M. Tijburg, *Preparation and properties of thermostable alumina-supported copper catalysts,* Thesis, University of Utrecht, 1989.
[2] H.J. Sloot, G.F. Versteeg and W.P.M. van Swaaij, A non-permselective membrane reactor for chemical processes normally requiring strict stoichiometric feed rates of reactants, *Chem. Eng. Sci., 45* (8) (1990) 2415–2421.
[3] J.W. Veldsink, R.M.J. van Damme, G.F. Versteeg and W.P.M. van Swaaij, A catalytically active membrane reactor for fast, exothermic, heterogeneously catalysed reactions, *Chem. Eng. Sci., 47* (9–11) (1992) 2939–2344.
[4] R.B. Anderson, K.C. Stein, J.J. Feenan and L.J.E. Hofer, Catalytic oxidation of methane, *Ind. Eng. Chem., 53* (10) (1961) 809–812.
[5] J. Malinsky, Katalytische verbrennung von Methan, *Erdöl und Kohle, 24* (1971) 82–84.
[6] D.L. Trimm, C.W. Lam, The combustion of methane on platinum–alumina fibre catalysts. I: Kinetics and mechanism, *Chem. Eng. Si., 35* (1980) 1405–1413.
[7] K. Georgakopoulos and R. Broucek, Investigation of the non-ideality of an internal recycle reactor using a concentration controlled test reaction, *Chem. Eng. Sci., 42* (11) (1987) 2782–2784.
[8] S. Wedel and J. Villadsen, Falsification of kinetic parameters by incorrect treatment of recirculation data, *Chem. Eng. Sci., 38* (8) (1983) 1346–1349.
[9] L.K. Doraiswamy and D.G. Tajbl, Laboratory catalytic reactors, *Cat. Rev. Sci. Eng., 10* (2) (1974) 177–219.
[10] G.F. Froment and K.B. Bischoff, *Chemical reactor analysis and design,* Wiley, New York, 1990.
[11] O.A. Hougen and K.M. Watson, *Chemical process principles, part 3: Kinetics and catalysis,* Wiley, New York, 1962.
[12] M.G. White, *Heterogeneous Catalysis,* Prentice-Hall, New Jersey, 1990.
[13] D.E. Mears, Diagnostic criteria for heat transport limitations in fixed bed reactors, *J. Catal., 20* (1971) 127–131.
[14] J.W. Butt and V.W. Weekman, Characterization of the activity, selectivity and aging properties of heterogeneous catalysis, *AIChE Symp. Ser., 143* (70) (1974) 27–41.
[15] W.J. Beek, *Proc. Int. Symp. Fluidization,* Netherlands University Press, Amsterdam, 1967, pp. 507–536.
[16] National Research Council of the United States of America, *International Critical Tables of Numerical data, physics, chemistry and technology,* McGraw-Hill, New York, 1933.
[17] W. Resnick and M. Golt, Particle-to-gas mass-transfer measurements and coefficients in fixed beds at low Reynolds numbers, *Int. J. Heat Mass Transfer, 24* (1981) 387–394.
[18] C.M. van den Bleek, K. van der Wiele and P.J. van den Berg, The effect of dilution on the degree of conversion in fixed bed catalytic reactors, *Chem. Eng. Sci., 24* (1969) 681–694.